Tetra-n-butylammonium decatungstate supported on Fe 3 O 4 nanoparticles: a novel nano-catalyst for green synthesis of nitroso compounds

Peng Cheng, Mohamed Sarakha, Christine Mousty, Pierre Bonnet, Gilles Mailhot

Tetra-n-butylammonium decatungstate supported on Fe_3O_4 nanoparticles: a novel nano-catalyst for green synthesis of nitroso compounds

*Peng Cheng, Mohamed Sarakha, Christine Mousty, Pierre Bonnet and Gilles Mailhot**

Université Clermont Auvergne, CNRS, Clermont Auvergne INP, Institut de Chimie de Clermont Ferrand (ICCF) UMR 6296, BP 80026, F-63171, Aubière cedex, France

* Corresponding author. E-mail address: Gilles.Mailhot@uca.fr.

Abstract

The aim of this study was to prepare a Fe_3O_4/tetra-n-butylammonium decatungstate (TBADT) catalyst (M-DT) for the selective oxidation of aromatic amine compounds in the presence of hydrogen peroxide (H_2O_2). The material M-DT, prepared from the interactions between TBADT and Fe_3O_4, was fully characterized by Fourier infrared spectroscopy (FTIR), X-ray diffraction (XRD), transmission electron microscopy (TEM), scanning electron microscopy (SEM), energy-dispersive X-ray spectroscopy (EDS) and, X-ray photoelectron spectroscopy (XPS). Electron transfers between H_2O_2 and TBADT or Fe_3O_4 or M-DT were studied by cyclic voltammetry (CV) using carbon-modified electrodes. The optimized M-DT/H_2O_2 catalytic system can effectively oxidize sulfapyridine (SPD) to nitroso-sulfapyridine (N-SPD) in the pH range of 2.5 to 4.6 with an efficient (93%) and selective conversion (86%). The oxidation rate constant (1.20×10^{-2} min^{-1}) is much higher with M-DT than with TBADT (2.09×10^{-4} min^{-1}) or Fe_3O_4 (4.81×10^{-4} min^{-1}) alone using 5 mM H_2O_2 as a co-catalyst. This M-DT catalyst can be reused 6 times with high efficiency and selectivity.

Keywords: TBADT; Fe_3O_4; H_2O_2; Amine oxidation; Electron transfer process.

1. Introduction

Nitroso compounds are known to be highly valuable chemical intermediates, which are versatile building blocks in polymer, dyes, agrochemicals, and pharmaceutical industries [1]. Nitroso compounds can be prepared easily from inexpensive starting materials [2]. Among the preparation methods, catalytic oxidation of primary amines appears to be one of the widely used methods [3–5]. In the last years, the most popular methodology to prepare nitroso compounds was the transition metal based catalyzed, with tungsten (W) [2,6], molybdenum (Mo) [1,7], vanadium (V) [7], zirconium (Zr) [8] and gold (Au) [9] as metals, in combination with H_2O_2. H_2O_2, known as a milder oxidant, is widely used in "green synthesis" since H_2O and O_2 represent the main reaction products [2,10]. However, the production of products such as azo or azo derivatives is the main reason for the low selectivity of this catalytic oxidation process [11]. Nowadays, improving the high activity and selectivity attracts more attention, and immobilization of transition metal catalysts on solid support became an interesting strategy [6,9]. Moreover, this catalyst has the potential to be recycled and reused several times. Tungstate catalysts proved to be efficient catalysts, for example, tungstate-supported silica-coated Fe_3O_4 nanoparticles prepared by Jadidi Nejad, et al. can be reused up to 6 times in presence of H_2O_2 to prepare nitroso compounds in a yield of roughly 70% [2].

Decatungstate (DT) is a catalyst commonly used for organic selective synthesis, especially in photo-catalyzed oxidation [12]. A variety of methods have been developed to prepare heterogeneous DT photocatalysts [12–16]. Considering the selection of the support material, a previous study proved that the interaction exists between iron oxide and tungstate oxide [17]. Rakshit et, al. proved that tungsten forms inner-sphere-type bonds on hematite surfaces using

in situ ATR-FTIR [18]. In addition, previous studies illustrated that this interaction can make the electron more easily transfer from W^{6+} sites to Fe^{3+} [17] and can be affected by pH [19].

Based on the well-comprehension of interaction between these two species, we sed, in the present study, nanoparticles of Fe_3O_4 (M) as a support of TBADT to synthesize a Fe_3O_4/TBADT (M-DT) composite material. We used M-DT to obtain a catalytic system to selectively oxidize sulfapyridine (SPD) to nitroso-sulfapyridine (N-SPD) in the presence of H_2O_2. Compared with tungstate-supported silica-coated Fe_3O_4 prepared by Jadidi Nejad, et al [2], the M-DT catalyst was innovatively prepared by directly linking TBADT on the Fe_3O_4 surface via the strong interaction between the W element and Fe element. Therefore, it is not necessary to coat the Fe_3O_4 with silica first, and the process of catalyst preparation is relatively simple. In addition, the mechanism research of this catalytic system is very interesting, and there are not many studies on the mechanism of this kind of catalytic system.

Hence, in this study, i) to investigate the mechanism of the M-DT/H_2O_2 catalytic system, the catalytic materials were characterized by XRD, FTIR, TEM, SEM, EDS, and XPS. The electron transfer between H_2O_2 and M-DT catalyst was studied by the CV experiment. ii) to identify the produced species, NMR, HPLC, and HRMs/UHPLC were used. iii) to optimize the efficiency and selectivity of the oxidation of the substrate to nitroso compound in the M-DT/H_2O_2 system, catalytic oxidation of SPD to N-SPD was investigated as a function of various parameters, such as the ratio of TBADT and Fe_3O_4 in M-DT, the amount of M-DT, the pH, and the concentrations of H_2O_2.

2. Experimental

2.1. Materials

Sulfapyridine (SPD) (≥ 99 %), sodium tungstate ($Na_2WO_4 \cdot 2H_2O$), tetra-n-butylammonium bromide (TBABr), hydrochloric acid (HCl), H_2O_2 (30%), perchloric acid ($HClO_4$), iron (III) chloride ($FeCl_3 \cdot 6H_2O$), iron(II) chloride ($FeCl_2 \cdot 4H_2O$) and sodium hydroxide (NaOH) were purchased from Sigma Aldrich and used without any further purifications. Water (Milli-Q) was purified using a reverse osmosis RIOS 5 and Synergy (Millipore) device. Its resistivity was 18 MΩ cm and the dissolved organic carbon (DOC) was estimated to be < 0.1 mg L^{-1}.

2.2. Preparation of TBADT, Fe_3O_4, and M-DT

The preparation of TBADT was performed using the method described elsewhere [20]. A boiling sodium tungstate solution (8 g of $Na_2WO_4 \cdot 2H_2O$ dissolved in 100 mL of ultrapure water) was added into 16.75 mL boiling hydrochloric acid (3.0 M). The temperature was maintained at 95 °C for 5 min till the color of the solution changed from colorless to green. Then, the addition of an aqueous solution (95 °C) of tetra-n-butylammonium bromide (TBABr 6.4 g/10 mL) leads to the immediate formation of a white precipitate. The mixture was kept under stirring at 95 °C for 5 min. This suspension was then filtered after cooling at ambient temperature. The solid was dissolved into dichloromethane, and then the solution was filtered to remove the insoluble particles. Finally, the obtained dichloromethane solution was gently evaporated at 38 °C to obtain the yellow-green catalyst. Nanoparticles of Fe_3O_4 were prepared by the procedure reported in the literature [21].

Fe_3O_4/TBADT solid, taking M-$DT_{2\text{-}1}$ as an example, was prepared by the following procedure. A mixture of 1.0 g TBADT and 2.0 g Fe_3O_4 was vigorously stirred in 10.0 mL acetonitrile. The reaction vessel was then kept in the dark for 20 hours at ambient temperature. After centrifugation, the solid was washed with Milli-Q water three times and

then dried in the oven at 50 °C. Different ratios of Fe_3O_4/TBADT (20/1, 10/1, 5/1, 2/1) were tested to prepare various M-DT using a similar process with an equivalent quantity of Fe_3O_4 (2.0 g).

2.3. Characterization

To characterize the purity of the synthesized TBADT, the UV-Vis absorption spectra of TBADT dissolved in acetonitrile (CH_3CN) were obtained using a Varian Cary 300 UV-vis spectrophotometer (**Fig. S1**). The X-ray diffraction (XRD) patterns of TBADT, Fe_3O_4, and M-$DT_{2\text{-}1}$ (before and after the reaction) were collected using an X-ray diffractometer (PANalytical X'Pert Pro) with a diffracted beam monochromator Cu Kα source (40 kV-40 mA). Patterns were recorded from 2θ = 5 to 70°, in steps of 0.08° with a count time of 4 seconds. The FTIR spectra of TBADT, Fe_3O_4, and M-$DT_{2\text{-}1}$ were recorded with Thermo-Nicolet 380 spectrometer with an advanced diamond ATR accessory (Specac-Golden Gate). For the characterization of the morphology and the size of particles of TBADT, Fe_3O_4, and M-$DT_{2\text{-}1}$, the samples were suspended in ethanol and dropped onto a 400-mesh holey carbon-coated copper grid and dried at room temperature, and then analyzed by transmission electron microscopy (TEM, Hitachi H-7650) at 80 kV acceleration voltage with magnifications up to 200×000. With the objective to check whether TBADT is uniformly covered on the surface of nano-Fe_3O_4, an element mapping experiment coupled with scanning electron microscopy analysis (SEM-EDS) was performed on a JEOL JSM-6490LV microscope. X-ray Photoelectron Spectroscopy (XPS) was performed on a Physical Electronics/PHI 5300 X-ray photoelectron spectrometer (S 250 Germany) with a hemispherical analyzer and a single-channel detector that was operated at 300W (15 kV and

20 mA). Mg Kα radiation (1253.6 eV) and pass energies of 89.45 eV for survey scans and 17.9 eV for high-resolution scans were used. The BET (Brunauer, Emmett, and Teller) surface area of the materials was determined by a Quantachrome Nova 3000e Surface Area Analyzer.

2.4. Catalytic tests: SPD oxidation

The conversion of SPD and the formation yield of its corresponding nitroso compound were performed in a batch experiment at room temperature (roughly 25°C). 20 mg M-DT was added into the 50 mL of SPD solution (30 μM). The pH of the solution was adjusted to 3.0 ± 0.05 using perchloric acid and sodium hydroxide (0.1 M). H_2O_2 was added using a known volume of a concentrated solution, and so with negligible volume, prior to starting the reaction using the magnetic stirrer at 1100 rpm min^{-1} to disperse Fe_3O_4 particles. Then, aliquots of the mixture were taken at different time intervals and were immediately filtrated using PTFE filters of 0.2 μm (CHROMAFIL® Xtra RC-20/25, 25 mm, Macherey-Nagel).

The effect of the ratio of Fe_3O_4/TBADT in M-DT (20/1, 10/1, 5/1, and 2/1), pH (1.9, 2.5, 3.0, 4.0, 4.6, 5.2, and 7.2), H_2O_2 concentration (1, 5, 10, 20, 30, 40, and 50 mM), and M-DT concentrations (0.1, 0.2, 0.4, and 1.2 g L^{-1}) was also investigated.

2.5. Preparative LC, UHPLC-MS, HPLC, and NMR Spectroscopy

Preparative liquid chromatography (LC) was used to separate and purify N-SPD from the reaction mixture. This separation was obtained using preparative LC (Varian Prep Star 218) equipped with a Varian Pro Star 335 photodiode array detector and an autosampler. The column was a C18 Varian Dynamax Microsorb 60-8 column (250 mm × 41.4 mm, 8 μm

particle size). The identification of all the byproducts was performed using high-resolution mass spectrometry (HRMS) constituted of an Orbitrap QExactive (Thermo Scientific) coupled to an ultra-high performance liquid chromatography (UHPLC) instrument Ultimate 3000 RSLC (Thermo Scientific). Analyses were carried out in both negative and positive electrospray modes (ESI^+ and ESI^-). The conversion of SPD and the formation of N-SPD percentages were obtained by HPLC (Shimadzu NEXERA XR HPL) equipped with a photodiode array detector and an auto-sampler. The column was a Macherey Nagel EC 150/2 NUCLEODUR C18ec (150 mm × 2 mm, 2 μm particle size). All the elution conditions of those LC are given in **SI**.

2.6. NMR spectroscopy

For the characterization and also quantification of the products, NMR spectroscopy was used. 100 μL at 5.22 mM of 3-(Trimethylsilyl) propionic acid-d_4 sodium salt ($TSPd_4$) in D_2O solution as a reference was added in 900 μL concentrated pure N-SPD solution. NMR data were obtained with a Bruker Advance Ⅲ 500 MHz Ultrashield^{TM} plus spectrometer (equipped with 5 mm TCI-13C-15N-2H Prodigy Cryoprobe). All spectra were recorded in 600 μL of H_2O (10% D_2O). Chemical shifts (δ) are expressed in ppm relative to the residual peak of 4.79 (ppm) of water.

2.7. Electrochemical measurement

Cyclic voltammetry (CV) experiments were carried out with a potentiostat Autolab PGSTAT204 controlled by the NOVA software (Metrohm) equipped with a three-electrodes system. An Ag-AgCl electrode was used as the reference electrode and a platinum wire as the

158 auxiliary electrode. The working electrodes were pyrolytic graphite electrodes (PGE, A =
159 0.07 cm^2) modified with a TBADT coating (**TBADT/PGE**), a Fe_3O_4 coating (**M/PGE**), and
160 an M-DT_{2-1} coating (**M-DT_{2-1}/PGE**) prepared by a solvent casting method. Before its use, the
161 PGE electrode surface was polished with 1 μm diamond paste and washed with acetone and
162 then it was polished again with 0.04 μm alumina slurry to be finally rinsed with ethanol and
163 water. To prepare the TBADT/PGE. 10 μL TBADT solution was deposited onto the polished
164 PGE and then air dried for 120 min. The M/PGE was also prepared using a solvent casting
165 method [22]. A suspension was prepared with 80 mg of Fe_3O_4 dispersed in 1.0 mL ethanol by
166 sonication for approximately 30 minutes. Then 10 μL Nafion solution (5%, Sigma Aldrich)
167 was added in the 1.0 mL Fe_3O_4 suspension followed by sonication for more than 15 min. 10
168 μL of the slurry was deposited onto the polished PGE and then air dried for 120 minutes.
169 Finally, for the M-DT/PGE, a suspension was prepared in a centrifuge tube with 40.0 mg of
170 TBADT and 80.0 mg of Fe_3O_4 (M-DT_{2-1}) dispersed in 1.0 mL acetonitrile for 24 hours on a
171 rotating reactor (45 rpm min^{-1}) at ambient temperature. After centrifugation, the solid was
172 washed with acetonitrile and Milli-Q water three times and then dry in the oven at 50 °C.
173 After getting the fresh M-DT, 1 mL ethanol was added in this centrifuge tube with sonication
174 for approximately 30 min, then 10 μL Nafion solution was added in the 1.0 mL M-DT_{2-1}
175 suspension followed by sonication for 30 min more. 10 μL of the slurry was deposited onto
176 the polished PGE and then air dried for 120 minutes. Cyclic voltammograms were recorded
177 with the TBADT/PGE, M/PGE or M-DT_{2-1}/PGE modified electrodes in a 0.1 M $LiClO_4$
178 electrolyte solution (at pH 3.5) in the presence or absence of H_2O_2 (5 mM) at a scan rate (v) of
179 10 mV s^{-1} under inert atmosphere. To avoid interference with O_2 reduction, the electrolyte

180 solution was bubbling with argon for 30 minutes prior to the CV experiments. The stability of
181 the modified electrodes was studied during several cycles, and the CVs shown corresponded
182 to the 10^{th} cycle. The recyclability of an M-DT/PGE electrode was also studied under the
183 same conditions, each time with a fresh $LiClO_4$ electrolyte solution.

184 **3. Results and discussion**

185 **3.1. Characterization of TBADT, Fe_3O_4, and M-DT_{2-1}**

186 Powder-XRD was used to characterize the solid compounds, Fe_3O_4, TBADT, and M-DT_{2-1}.
187 As shown in **Fig. 1**, the XRD pattern of Fe_3O_4 (**curve a**) presents several diffraction lines at
188 $2\theta = 18.44°$, 30.30°, 35.67°, 37.18°, 43.32°, 53.78°, 57.29°, 62.95°. These are in perfect
189 agreement with those reported in a standard pattern of PDF-#89-6466 (Shown in **Fig. 2**)
190 leading us to the conclusion that Fe_3O_4 is successfully synthesized. The **curve b** represents
191 the XRD pattern of TBADT, which shows two significant peaks at 7.33° and 7.62° and
192 several small peaks from 5° to 40°, which is quite similar to the previous study [23]. For the
193 XRD pattern of M-DT_{2-1} **(curve c**), the characteristic peaks of Fe_3O_4 and TBADT can be
194 observed, which means TBADT is successfully attached to the surface of Fe_3O_4 particles. In
195 addition, the intensity of TBADT in M-DT_{2-1}, after it has been used as a catalyst in the
196 oxidation reaction (**curve d**), does not decrease, which seems to indicate that the
197 immobilization of TBADT is quite stable on the surface of Fe_3O_4. While the interaction
198 between Fe_3O_4 and TBADT is not shown in XRD patterns, further characterizations by FTIR
199 and XPS are performed, and the results are presented in the **SI** file (**Fig S2, S3, Tables S1,**
200 **S2, and S3**). These results illustrate that there is a strong interaction between TBADT and

Fe_3O_4, moreover, the chemical composition of Fe_3O_4 has not significantly changed after M-DT_{2-1} synthesis and after the reaction.

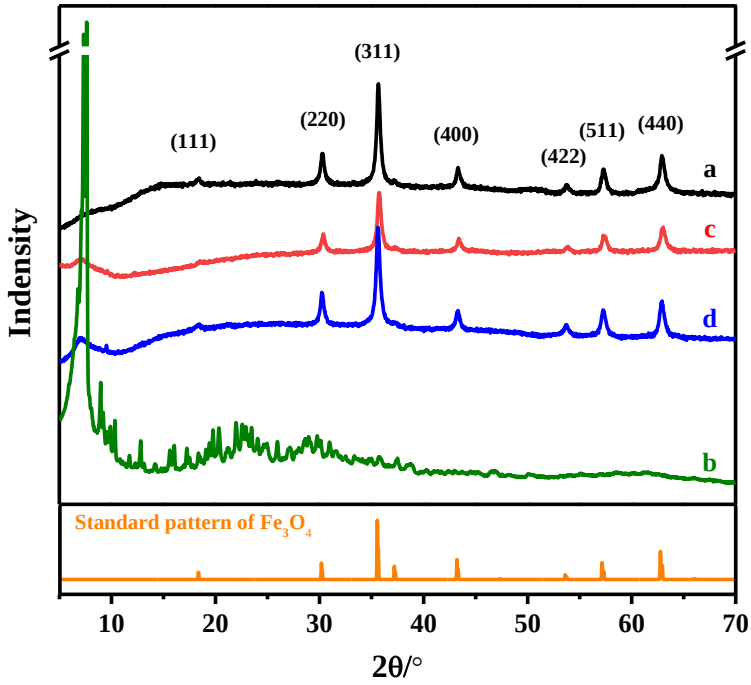

Fig. 1. XRD patterns of Fe_3O_4 (a), TBADT (b), M-DT_{2-1} before (c) and after reaction (d)

The morphology and particle sizes of those materials were analyzed by TEM. **Fig. S4** shows the TEM images of Fe_3O_4 (a), TBADT (b), and the M-DT_{2-1} before (c) and after reaction (d). Fe_3O_4 has a globosity morphology with particle diameters ranging from 20 to 40 nm. This leads us to the conclusion that we are dealing with a nano-Fe_3O_4 material which presents more likely a large surface area (BET surface area = 74 ± 1 m^2 g^{-1}). TBADT presents a short rod-like morphology with a length of 100 nm (**Fig. S4(b)**). The morphology of M-DT_{2-1} is very similar to the morphology of Fe_3O_4, the short rod-like TBADT is not observed in the M-DT_{2-1}. This is because in the preparation process of the M-DT_{2-1}, TBADT is first dissolved in acetonitrile, and then individual clusters of TBADT will be wrapped on the surface of the Fe_3O_4 through an inner-sphere type bond. In addition, the morphology of

M-DT_{2-1} does not change after the reaction (**Fig. S4(c)**), which confirms that the M-DT_{2-1} has a certain degree of durability.

To verify whether TBADT is uniformly covered on the surface of nano-Fe_3O_4, SEM-EDS element mapping technology is used to visually study the distribution of elements. **Fig. 2** shows the SEM image and SEM-EDS element mapping of M-DT_{2-1} before and after the reaction. The elements such as Fe and W have the same distribution both in the M-DT_{2-1} before and after the reaction, indicating that TBADT is evenly distributed on the surface of nano-Fe_3O_4. After overlapping the W and Fe distribution images, we can infer that M-DT_{2-1} has a core-shell structure with Fe_3O_4 as the core and TBADT wrapped in the outer layer. In addition, after the catalytic reaction, the amount of W element does not decrease (about 3 atomic percent, shown in **Fig. 2**), which confirmed the stability of the M-DT_{2-1} catalyst.

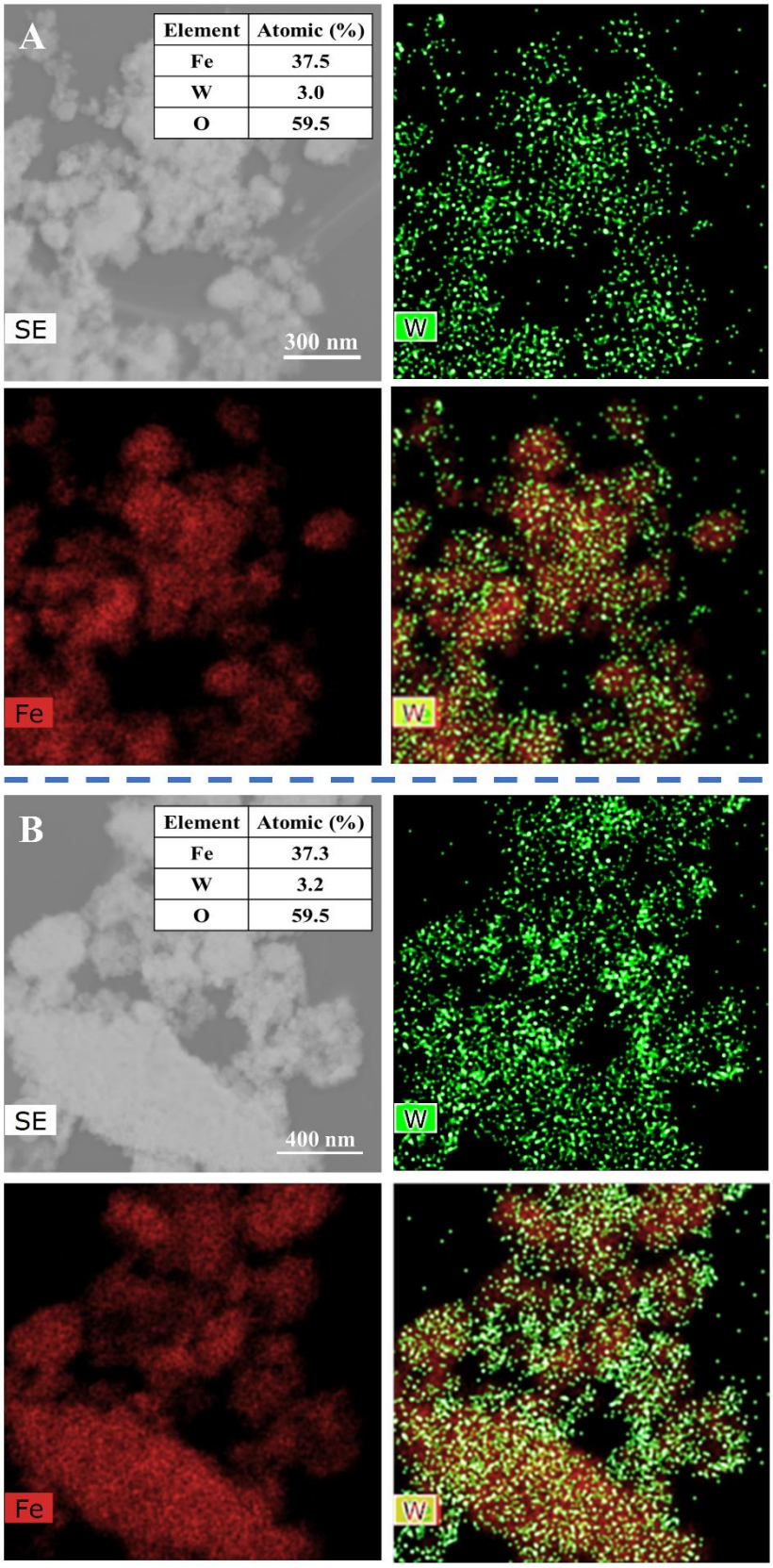

Fig. 2. SEM image and SEM-EDS element mapping of M-$DT_{2\text{-}1}$ before (A) and after reaction (B).

3.2. Electrochemical behavior of TBADT, Fe_3O_4, and M-DT_{2-1}

To study the possible electron transfer between those materials and H_2O_2, we have compared the electrochemical behavior of TBADT deposited on a pyrolytic carbon electrode (**TBADT/PGE**), Fe_3O_4 modified electrode (**M/PGE**), and the composite M-DT_{2-1} modified electrode (**M-DT_{2-1}/PGE**) in the absence and the presence of H_2O_2 by CV experiment.

Fig. 3 shows cyclic voltammograms of TBADT/PGE (A) and M-DT_{2-1}/PGE (B) in the absence and presence of H_2O_2. The dashed line represents the baseline recorded at the bare PGE in 0.1 mM $LiClO_4$ electrolyte at pH 3.5 under argon, showing no interference with oxygen reduction.

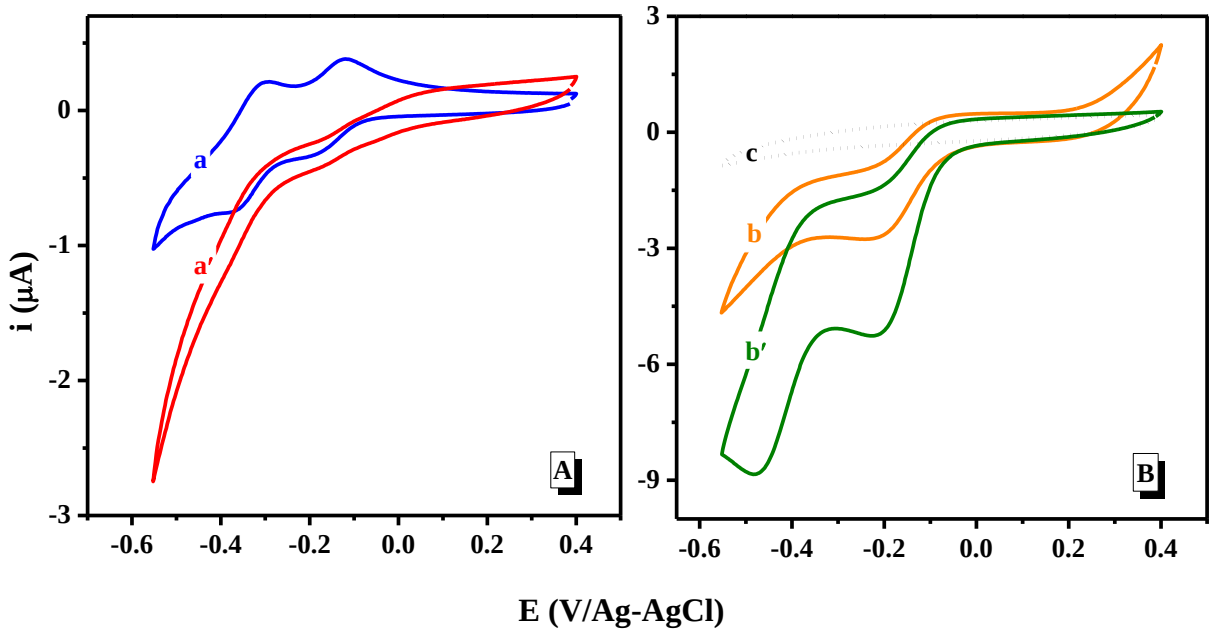

Fig. 3. Cyclic voltammograms of A) TBADT/PGE and B) M-DT_{2-1}/PGE in the absence (a and b) or presence of 5 mM H_2O_2 (a′, b′) in 0.1 M $LiClO_4$ (pH = 3.5) under Ar, v = 10 mV s^{-1}. The dashed line (curve c) corresponds to the PGE baseline in 0.1 M $LiClO_4$ pH 3.5 under Ar.

The CV of TBADT/PGE (**Fig. 3(A), curve a**) exhibits two reversible signals. The potential

of the first cathodic peak (Ep_{c1} = -0.18 V/Ag-AgCl) and the second one (Ep_{c2} = -0.37 V/Ag-AgCl) are consistent with the values reported in the literature for sodium decatungstate (NaDT) in aqueous solution [24,25], while Yang, et al reported the first cathodic at 0.06 V/SCE for TBADT dissolved in a mixed solvent (10% HCl (12 M) + 90 % CH_3CN) [26], which is due to the different polarity of the solvent [27]. The peak separation ($\triangle E = Ep_c - Ep_a$) is 60 mV for the first and the second redox couples, showing good reversibility of the electron transfer which can be assigned to the following reactions:

$$W_{10}O_{32}^{4-} + H^+ + e^- \rightleftharpoons HW_{10}O_{32}^{4-} \qquad (1)$$

$$HW_{10}O_{32}^{4-} + H^+ + e^- \rightleftharpoons H_2W_{10}O_{32}^{4-} \qquad (2)$$

Curve **a′** in **Fig. 3(A)** corresponds to the electrochemical signal of TBADT in the presence of 5 mM H_2O_2. The shape of the voltammograms changes when H_2O_2 is added to the electrolyte solution. Although the two cathodic peaks are not obvious, the current intensity of these two peaks seems to increase slightly (current at Ep_{c1}= -0.18V and Ep_{c1}= -0.37V are -0.43 μA and-1.10 μA, respectively), while the corresponding anodic peak current decreases.

Curve b in Fig. 3(B) represents the CV of the M-$DT_{2\text{-}1}$/PGE in 0.1 mM $LiClO_4$ electrolyte at pH 3.5 under argon. A cathodic peak can be observed at Ep_{c1} = -0.23 V/Ag-AgCl (I_{c1} = -2.77 μA). The presence of H_2O_2 in the electrolyte causes an increase of the cathodic current (Ip_{c1} × approximately 2 times) and the appearance of a second irreversible peak at Ep_{c2} = -0.48 V/Ag-AgCl (**curve b′**). The shape of those catalytic waves is similar to those we have previously reported using M/PGE and NaDT in solution. Even if the peak intensities cannot be compared directly, since the same amount of DT was not deposited on both electrode surfaces, it was notable that the catalytic current obtained in the presence of H_2O_2 at

M-$DT_{2\text{-}1}$/PGE was much higher than the one recorded at the TBADT/PGE. This indicates that there is an interaction between TBADT and Fe_3O_4 leading to an enhancement of the electrocatalytic process.

For comparison, **Fig. S5** shows the CVs recorded using a M/PGE with and without 5.0 mM H_2O_2 added to the electrolyte solution. With M/PGE, a well-defined cathodic peak is observed at -0.08 V which is owing to an electro-Fenton process occurring at the Fe_3O_4 surface [28,29]. This process can be expressed by equations (3 and 4):

$$Fe^{3+} + e^- \rightarrow Fe^{2+} \qquad (3)$$

$$Fe^{2+} + H_2O_2 \rightarrow Fe^{3+} + {}^{\bullet}OH + OH^- \qquad (4)$$

However, in this case, the catalytic current (Ip_c = 2.05 μA) is lower than with M-$DT_{2\text{-}1}$/PGE. This means that with M-$DT_{2\text{-}1}$ particles on the electrode surface, the electrocatalytic process for H_2O_2 reduction is definitively improved. The mechanisms of these electrocatalytic processes are probably not the same on both types of the electrode (M/PGE and M-$DT_{2\text{-}1}$/PGE), implying in the latter case, iron species from Fe_3O_4 in interaction with TBADT, as suggested by Dong and Liu for Dawson-type tungstatephosphonate anion [30].

The current stability of M-$DT_{2\text{-}1}$/PGE was investigated in the CVs experiment in the absence (A) and presence of H_2O_2 (B) for 10 potential cycles (**Fig. S6).** In absence of H_2O_2, a cathodic peak at -0.18 V/Ag-AgCl (Ip_{c1}= -7.87 μA) can be observed in the first cycle, and then the signal is stabilized with the cathodic peak Ep_{c1} at -0.23V/Ag-AgCl and Ip_{c1} = 2.3μA. The higher current in the first cycle may be due to the reduction of some O_2 molecules adsorbed on the modified electrode. In the presence of H_2O_2, the current stabilized also rapidly, showing that the M-$DT_{2\text{-}1}$ coating on the PGE surface is relatively stable. The

appearance of the second cathodic peak (Ep_{c2}) seems to be limited by diffusion restrictions through the film that seems to be solved after 2 or 3 cycles.

To investigate the recycling performance of the M-DT_{2-1}, the same M-DT_{2-1}/PGE was used to perform the CVs experiment six times in a fresh electrolyte solution under Ar in the presence of 5.0 mM H_2O_2 (**Fig. S7)**. The second cathodic peak (Ep_{c2}) can be seen after the second use, which is consistent with the above result. Insert shows the evolution of the cathodic current (Ip_{c1} and Ip_{c2}) as a function of the electrode uses confirming the good reproducibility of the electrocatalytic process occurring at the M-DT_{2-1}/PGE electrode. This result indicates that the W element did not decrease after the reaction as well.

3.3. Investigation of the catalytic performance

3.3.1 Comparison of the oxidation process in different systems

The synthesized M-DT composite material associated with H_2O_2 was used to oxidize SPD and the efficiency was evaluated. With this objective, an aqueous solution of SPD at a concentration of 30.0 μM was mixed first with M-DT_{2-1} and H_2O_2 (5.0 mM) at pH = 3.0. For the sake of comparison, experiments were also performed with H_2O_2 alone, Fe_3O_4/H_2O_2, and TBADT/H_2O_2 under the same experimental conditions. **Fig. 4** shows that in the presence of H_2O_2 alone (5.0 mM), almost no oxidation SPD (<1.5% within 2 hours) was obtained under our experimental conditions. Within the same time, the conversion was estimated to be 0.4 % with TBADT/H_2O_2 (0.4 g L^{-1}/5.0 mM) and 9.3 % with Fe_3O_4/H_2O_2 (0.4 g L^{-1}/5.0 mM). However, in the presence of 0.4 g L^{-1} synthetized M-DT_{2-1} and 5.0 mM of H_2O_2, the conversion reachs 75.8 % within 120 minutes, demonstrating the important and interesting

oxidation ability of the M-$DT_{2\text{-}1}$/H_2O_2 system toward SPD. Under our experimental conditions, the conversion appears to follow first-order kinetics and the rate constant is estimated to be 1.20×10^{-2} min^{-1}. While performing the experiments in the absence of H_2O_2, we can easily evaluate the SPD adsorption ability of the solid support. As shown in **Fig. S8** no adsorption of SPD is observed on TBADT, Fe_3O_4, and M-$DT_{2\text{-}1}$ within 2 hours.

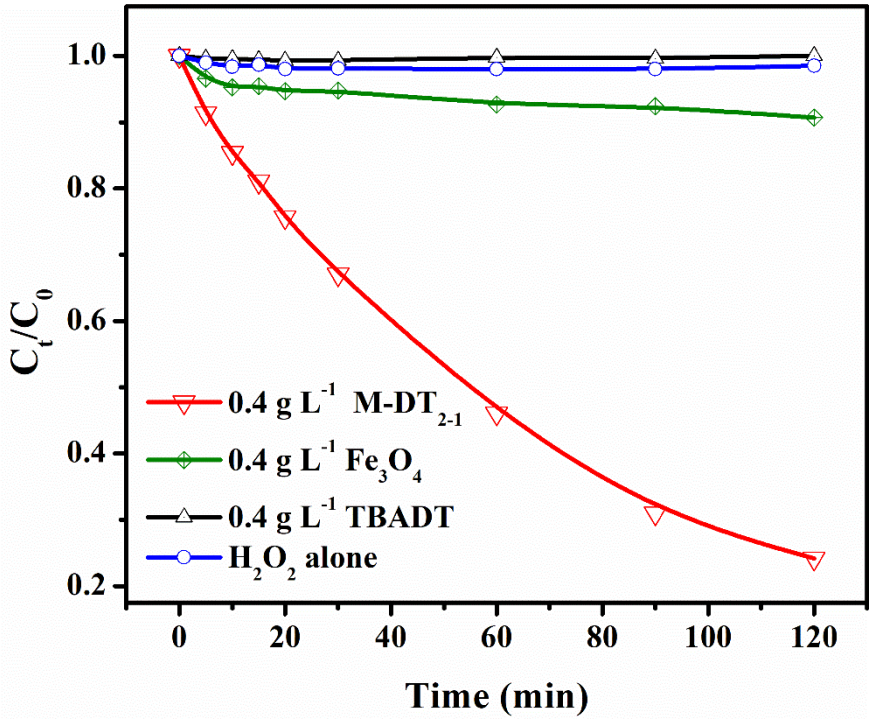

Fig. 4. Kinetics of SPD disappearance under various experimental conditions, [SPD] = 30 μM; H_2O_2 = 5.0 mM; pH = 3.0

The generated products in the M-$DT_{2\text{-}1}$/H_2O_2 systems were analyzed by HRMs/UHPLC and NMR. The disappearance of SPD leads to the formation of mainly three products among them the N-SPD ($m/z_{[M+H+]}$ = 264.0435 (**Table S4**) and, the hydroxyl-sulfapyridine (SPD-OH) product (**P1**) which is mainly formed in Fe_3O_4/H_2O_2 system, more likely owing the classical Fenton and Fenton-like processes [31]. On a contrary, the N-SPD is the main product formed in the M-$DT_{2\text{-}1}$/H_2O_2 system leading us to the conclusion that the simultaneous presence of

Fe_3O_4 and TBADT greatly promotes the amino selective oxidation into nitroso compound. The NMR spectrum confirms this result (**Fig. S9**). The quantification of N-SPD is performed by using the NMR technique according to the procedure given in **SI**. The average concentration of N-SPD calculated after quantification by NMR is 52.03 μM (Dropping a sample with a chemical shift of 7.93 ppm), and the relative standard deviation is (**RSD**) 4.8% (**Table S5)**.

3.3.2. The effect of different parameters

To optimize such oxidation process of SPD, the effect of various ratios of Fe_3O_4/TBADT (**Table S6**), pH (**Table S7**), the concentration of H_2O_2 (**Table S8**), and amount of M-DT_{2-1} (**Table S9**) were investigated.

The obtained results demonstrate that the SPD conversion percentage increases from 7.8 to 51.5% with the increase of the percentage of TBADT in M-DT from 4.8% to 33.3% (**Fig. S10**). For the coming experiments, M-DT with a ratio of 2/1 which is marked as M-DT_{2-1} was chosen. The pH can affect the conversion of SPD to N-SPD, the efficiency of SPD conversion decreases with the increase of the solution pH (**Fig. S11)**. Meanwhile, the conversion percentage of SPD decreases also when the pH increases**.** These are more likely due to the lower stability of decatungstate at pH > 5.5, and also due to the interaction between Fe and W decreasing when pH increases [18]. As the H_2O_2 concentration increases from 0 to 20 mM, the conversion rate and rate constant of SPD oxidation increase (**Fig. S12**), however those values both decrease with the H_2O_2 concentration increase from 20 to 50 mM. For the amount of M-DT_{2-1}, the conversion rate and rate constant of SPD oxidation increase and reach a plateau

when increasing the amount of M-DT_{2-1} (**Fig. S13**). The yield of N-SPD increases and reaches a plateau when H_2O_2 and the amount of M-DT_{2-1} increase.

3.3.3. Recycling experiments

To demonstrate that synthesized M-DT_{2-1} can be recycled, it was collected after each reaction and reemployed for the same experiments. **Table 1** shows the conversion of SPD and selectivity for the formation of N-SPD in this system during repeated experiments. The SPD conversion and the yield of N-SPD formation remain between 90.5 - 94.5% and 77.6 - 79.4% in 5 times repeated experiments, respectively. A small decrease in the conversion efficiency can be observed according to the rate constant and percentage of SPD disappearance which may be due to the loss of TBADT on the Fe_3O_4 surface. However, the yield of N-SPD formation remains at a high level. This indicates that the M-DT_{2-1} is a highly efficient catalyst material that can be reused and is likely to be used in actual production in the future.

Table 1 The conversion and selectivity of SPD in repeated experiments within 2h

Number of cycles	1	2	3	4	5
Rate constant ($\times 10^{-3}$ min^{-1})	22.5	21.3	21.8	21.3	20.5
Percentage of SPD disappearance (%)	93.4%	94.5%	92.7%	91.6%	90.5%
The yield of N-SPD formation (%)	78.7%	77.9%	79.4%	78.6%	77.6%

[M-DT_{2-1}] = 0.8 g L^{-1}; [H_2O_2] = 5.0 mM; [SPD] = 30 μM; pH = 3.0;

3.4. Comparison of catalytic performance

To understand the work of selective catalysis more deeply, we have compared systematically the results of selective oxidation of SPD using sodium decatungstate (NaDT)

and TBADT associated with Fe_3O_4. **Table 2** shows the SPD selective oxidation reaction parameters in NaDT/M/H_2O_2 and M-$DT_{2\text{-}1}$/H_2O_2 systems. It is observed that the catalytic performance for the selective oxidation of SPD, such as the rate constant of SPD disappearance ($\times 10^{-3}$ min^{-1}), the percentage of SPD disappearance (%), and the yield of N-SPD formation (%) shows no significant difference, when the reaction parameters, such as the concentration of decatungstate, Fe_3O_4, H_2O_2, SPD, and pH are the same in above mentioned both systems. In addition, the optimal parameters of the reaction have similarities. For example, the optimal pH for both systems is in the range of 2.5 - 4.0, and the optimal concentration of H_2O_2 is in the range of 5.0 - 20.0. These similarities can let us infer that the two systems have the same reaction mechanism.

However, it should be noted that the amount of catalyst (NaDT and TBADT) that interacted on the Fe_3O_4 surface is different, around 15.4 μM g^{-1} of TBADT/M and 74.1μM g^{-1} of NaDT/M were adsorbed on the Fe_3O_4 surface (**Fig. S14**), but the SPD oxidation and N-SPD formation efficiency are the same. This result indicates that the M-$DT_{2\text{-}1}$/H_2O_2 system is about 5 times more efficient than NaDT/M/H_2O_2 system.

The catalytic performance of M-$DT_{2\text{-}1}$/H_2O_2 systems was also compared with previous studies in the two dimensions of substrate conversion rate and selectivity. As shown in **Table. S10**, M-$DT_{2\text{-}1}$/H_2O_2 system has good and green catalytic performance in aqueous solution with high oxidation efficiency (97% conversion rate) and high selectivity (85% yield of N-SPD).

Table 2. The comparison of selective oxidation parameters using soluble and insoluble DT Synergistic Fe_3O_4 and H_2O_2 Systems

System	$NaDT/Fe_3O_4/H_2O_2$ System	$M\text{-}DT_{2\text{-}1}/H_2O_2$ System
$[W_{10}O_{32}^{4-}]$ (μM)	41 (NaDT)	40.2 (TBADT)
$[W_{10}O_{32}^{4-}]$ on the surface (μM g^{-1})	74.1	15.4
$[Fe_3O_4]$ (g L^{-1})	0.264	0.266
$[H_2O_2]$ (mM)	5.0	5.0
[SPD] (μM)	30	30
pH	3.0	3.0
Rate constant ($\times 10^{-3}$ min^{-1})	11.3	12.0
Percentage of SPD disappearance (%)	75.4	75.8
The yield of N-SPD formation (%)	71.3	73.8

3.5. Mechanistic study

The obtained results demonstrate that the oxidation of SPD into N-SPD is efficient at a pH lower than 5.0 using an $M\text{-}DT_{2\text{-}1}/H_2O_2$ catalyst. The rate constant and the percentage of SPD disappearance and the yield of N-SPD formation overall increase when concentrations of $M\text{-}DT_{2\text{-}1}$ and H_2O_2 increase. The characterization results and CV experiments analysis clearly show that there is an interaction between Fe_3O_4 and TBADT. The mechanism in $M\text{-}DT/H_2O_2$ system could be explained by an electron transfer from the amine site of SPD to TBADT giving rise to the formation of the reduced species TBADT with the simultaneous formation of the radical cation $[Ar\text{-}NH_2]^{\bullet+}$. The radical cation $[Ar\text{-}NH_2]^{\bullet+}$ further reacts with H_2O_2 to form N-SPD owing to the interaction between W and Fe atom, the electron can efficiently

transfer to Fe_3O_4. At the same time, the Fe^{3+} on the surface becomes Fe^{2+}, and the regeneration of Fe^{3+} happens in presence of H_2O_2 in the solution. The formation of SPD-OH is a sign of hydroxyl radical formation. This could be produced via a Fenton reaction. The efficiency of the process is mainly owing to the interaction of TBADT with M particles (**Scheme. 1**)

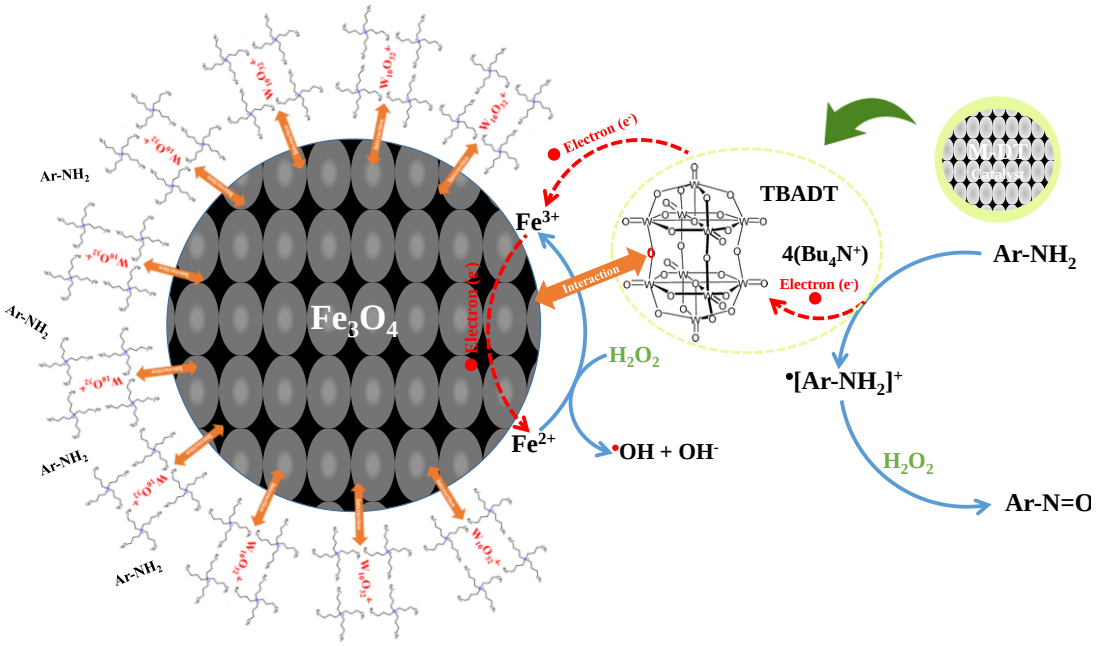

Scheme 1. Proposed mechanism for the selective oxidation process of primary aromatic amines to nitroso aromatic compounds using the M-DT/H_2O_2 catalytic system

4. Conclusions

The heterogeneous M-DT/H_2O_2 system (TBADT/Fe_3O_4/H_2O_2) appears to be a powerful system for the efficient (until 93%) and selective conversion (until 85%) of amine substrates to their nitroso derivatives. The system consists of a composite material M-DT obtained through interaction between Fe_3O_4 and TBADT as clearly demonstrated by several characterizations and CV experiments. This interaction is without any doubt the driving force

for the electron transfer implied in the catalytic process, leading to the formation of the radical cation on the amine group and the reduced species of TBADT. The regeneration of the $W_{10}O_{32}^{4-}$ is obtained via a second electron transfer with Fe_3O_4 owing to the interaction. Thus, in this study, we demonstrated that the system M-DT/H_2O_2 is an innovative and powerful catalytic system leading to a high yield of transformation for the generation of nitroso compounds from the amine group. It could be used and implemented easily for the synthesis of such chemical compounds in different applications.

Conflicts of interest

There are no conflicts to declare.

Acknowledgement

Peng CHENG thanks the Chinese scholarship council for its financial support (CSC201806690001) and thanks professor Marcello BRIGANTE, engineers Guillaume VOYARD, David BOURGOGNE and Aurélie JOB; and doctor Yara ARBID for their help in some experiments.

Reference

1 A. V. Biradar, T. V. Kotbagi, M. K. Dongare and S. B. Umbarkar, *Tetrahedron Letters*, 2008, **49**, 3616–3619.

2 M. Jadidi Nejad, E. Yazdani, M. Kazemi Miraki and A. Heydari, *Chem. Pap.*, 2019, **73**, 1575–1583.

3 R. R. Holmes and R. P. Bayer, *J. Am. Chem. Soc.*, 1960, **82**, 3454–3456.

4 B. G. Gowenlock and W. Lüttke, *Q. Rev. Chem. Soc.*, 1958, **12**, 321–340.

5 Y. Shiraishi, H. Sakamoto, K. Fujiwara, S. Ichikawa and T. Hirai, *ACS Catal.*, 2014, **4**, 2418–2425.

6 P. L. Gkizis, I. Kalara-Lafkioti, D. Varelas, I. Tamiolakis, G. S. Armatas and I. N. Lykakis, *Biointerface Research in Applied Chemistry*, 2014, **4**, 857–860.

7 V. Conte and B. Floris, *Dalton Trans.*, 2011, **40**, 1419–1436.

8 K. Krohn, *Synthesis*, 1997, **1997**, 1115–1127.

9 S. Fountoulaki, P. L. Gkizis, T. S. Symeonidis, E. Kaminioti, A. Karina, I. Tamiolakis, G. S. Armatas and I. N. Lykakis, *Advanced Synthesis & Catalysis*, 2016, **358**, 1500–1508.

10 M. M. Heravi, N. Ghalavand and E. Hashemi, *Chemistry*, 2020, **2**, 101–178.

11 D. Zhao, M. Johansson and J.-E. Bäckvall, *European Journal of Organic Chemistry*, 2007, **2007**, 4431–4436.

12 L. Pasti, E. Sarti, A. Martucci, N. Marchetti, C. Stevanin and A. Molinari, *Applied Catalysis B: Environmental*, 2018, **239**, 345–351.

13 M. D. Tzirakis, I. N. Lykakis, G. D. Panagiotou, K. Bourikas, A. Lycourghiotis, C. Kordulis and M. Orfanopoulos, *Journal of Catalysis*, 2007, **252**, 178–189.

14 A. Molinari, A. Bratovcic, G. Magnacca and A. Maldotti, *Dalton Trans.*, 2010, **39**, 7826–7833.

15 P. J. Sarver, V. Bacauanu, D. M. Schultz, D. A. DiRocco, Y. Lam, E. C. Sherer and D. W. C. MacMillan, *Nat. Chem.*, 2020, **12**, 459–467.

16 L. Ni, J. Ni, Y. Lv, P. Yang and Y. Cao, *Chem. Commun.*, 2009, 2171–2173.

17 H. Wang, Z. Qu, S. Dong, H. Xie and C. Tang, *Environ. Sci. Technol.*, 2016, **50**, 13511–13519.

18 S. Rakshit, B. Sallman, A. Davantés and G. Lefèvre, *Chemosphere*, 2017, **168**, 685–691.

19 B. Sallman, S. Rakshit and G. Lefèvre, *Chemosphere*, 2018, **213**, 596–601.

20 H. Li, X. Jiang, W. Zhu, J. Lu, H. Shu and Y. Yan, *Ind. Eng. Chem. Res.*, 2009, **48**, 9034–9039.

21 W. Huang, M. Luo, C. Wei, Y. Wang, K. Hanna and G. Mailhot, *Environmental Science and Pollution Research*, 2017, **24**, 10421–10429.

22 H. Liu, Q. Chen, X. Cheng, Y. Wang, Y. Zhang and G. Fan, *Sensors and Actuators B: Chemical*, 2020, **314**, 128067.

23 A. Su, M. Chen, Z. Fu, B. Yang, J. She, F. Wan, C. Zhang and Y. Liu, *Inorg. Chem.*, 2020, **59**, 7520–7530.

24 I. Moriguchi and J. H. Fendler, *Chem. Mater.*, 1998, **10**, 2205–2211.

25 S. C. Termes and M. T. Pope, *Inorg. Chem.*, 1978, **17**, 500–501.

26 B. Yang, Z. Fu, A. Su, J. She, M. Chen, S. Tang, W. Hu, C. Zhang and Y. Liu, *Applied Catalysis B: Environmental*, 2019, **242**, 249–257.

27 A. V. Kozytskiy, Y. V. Panasyuk and A. M. Mishura, *Theoretical and Experimental Chemistry*, 2018, **54**, 322–330.
28 P. V. Nidheesh and R. Gandhimathi, *Desalination*, 2012, **299**, 1–15.
29 E. Brillas, I. Sirés and M. A. Oturan, *Chem Rev*, 2009, **109**, 6570–6631.
30 S. Dong and M. Liu, *Journal of Electroanalytical Chemistry*, 1994, **372**, 95–100.
31 Y. Zhang and M. Zhou, *Journal of Hazardous Materials*, 2019, **362**, 436–450.